Engineering Fracture Mechanics Vol. 35, No. 4/5, pp. 665–677, 1990
Printed in Great Britain.

0013-7944/90 $3.00 + 0.00
Pergamon Press plc.

FRACTURE OF REINFORCED CONCRETE: SCALE EFFECTS AND SNAP-BACK INSTABILITY

C. BOSCO, A. CARPINTERI and P. G. DEBERNARDI

Department of Structural Engineering, Politecnico di Torino, Corso Duca degli Abruzzi, 24, 10129 Torino, Italy

Abstract—Remarkable size-scale effects are theoretically predicted and experimentally confirmed in low reinforced high strength concrete beams. The brittleness of the system increases by increasing size-scale and/or decreasing steel area. On the other hand, a physically similar behaviour is revealed in the cases where the non-dimensional number:

$$N_P = \frac{f_y \cdot b^{1/2}}{K_{IC}} \cdot \frac{A_S}{A}$$

is the same, f_y being the steel yield strength, K_{IC} the concrete fracture toughness, b the beam depth and A_S/A the steel percentage. The tensile strength and toughness of concrete, usually disregarded, are so high in some cases that the peak bending moment overcomes the bending moment of limit design (hyperstrength). The drop in the loading capacity can hide a virtual softening branch with positive slope (snack-back), which is detected if the loading process is controlled through the crack width.

1. INTRODUCTION

WHEN A small percentage of steel is required to reinforce high strength concrete, the crushing failure of the beam edge in compression is usually avoided. On the other hand, one or more cracks originate at the beam edge in tension and the material is so brittle in this case that the size of the crack tip process zone is very small if compared with the size of the zone where the stress singularity field is dominant. For these reasons, it will be shown that a Linear Elastic Fracture Mechanics model[1–3] is able to capture the most relevant aspects and trends in the mechanical and failure behaviour of low reinforced high strength concrete beams in flexure.

The present theoretical and experimental investigation aims at evaluating the size-scale effects on reinforced concrete members, by means of three point bending tests. Thirty (30) R.C. beams are tested, with thickness $t = 150$ mm and depth $b = 100$, 200, 400 mm, respectively. The span is assumed to be six times the beam depth b.

Five different values of the non-dimensional number

$$N_P = \frac{f_y \cdot b^{1/2}}{K_{IC}} \cdot \frac{A_S}{A}$$

are considered (about equal to 0.00, 0.10, 0.30, 0.75, 1.20), f_y being the steel yield strength, K_{IC} the concrete fracture toughness and A_S/A the steel percentage. Both size-scale b and steel percentage A_S/A are varied. The ratio of the distance of the bars from the lower edge of the beam, to the beam depth is assumed to be constant and equal to 0.1.

The loading process is carried out on initially uncracked R.C. beams, by controlling the tensile strain on the lower edge of the beam or, after cracking, the crack mouth opening displacement. Even the compressive strain on the upper edge of the beam and the beam deflection are recorded.

Remarkable size-scale effects are theoretically predicted and experimentally confirmed. The brittleness of the system increases by increasing size-scale and/or decreasing steel area. On the other hand, a physically similar behaviour is revealed in the cases where the non-dimensional number N_P is the same.

The phenomena of catastrophical softening (snap-back) and hyperstrength in low reinforced concrete beams are interpreted according to the concepts of Fracture Mechanics. The tensile strength and toughness of concrete, usually disregarded, are so high in some cases that the ultimate bending moment overcomes the bending moment of limit design. The drop in the loading capacity can hide a virtual softening load–deflection branch with positive slope, which is detected if the

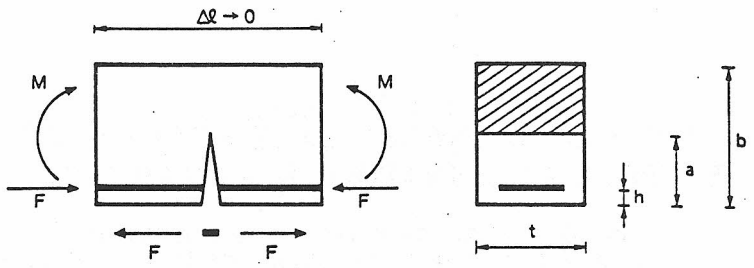

Fig. 1. Cracked concrete beam element.

loading process is controlled through the crack width. In this way, a phenomenon unstable in nature is made stable in practice[4–6].

2. THEORETICAL MODEL

Let the cracked concrete beam element in Fig. 1 be subjected to the bending moment M and to an eccentric axial force F due to the statically undetermined reaction of the reinforcement. It is well-known that bending moment M^* and axial force F^* induce stress-intensity factors at the crack tip respectively equal to[7, 8]:

$$K_I^{(M)} = \frac{M^*}{b^{3/2} \cdot t} \cdot Y_M(\xi) \tag{1a}$$

$$K_I^{(F)} = \frac{F^*}{b^{1/2} \cdot t} \cdot Y_F(\xi) \tag{1b}$$

where Y_M and Y_F are given, for $\xi = a/b \leqslant 0.7$, by:

$$Y_M(\xi) = 6(1.99\,\xi^{1/2} - 2.47\,\xi^{3/2} + 12.97\,\xi^{5/2} + 23.17\,\xi^{7/2} + 24.80\,\xi^{9/2}) \tag{1c}$$

$$Y_F(\xi) = (1.99\,\xi^{1/2} - 0.41\,\xi^{3/2} + 18.70\,\xi^{5/2} - 38.48\,\xi^{7/2} + 53.85\,\xi^{9/2}). \tag{1d}$$

On the other hand, M^* and F^* produce local rotations, respectively, equal to[7, 8]:

$$\phi^{(M)} = \lambda_{MM} \cdot M^* \tag{2a}$$

$$\phi^{(F)} = \lambda_{MF} \cdot F^* \tag{2b}$$

where

$$\lambda_{MM} = \frac{2}{b^2 \cdot t \cdot E} \cdot \int_0^\xi Y_M^2(\xi)\,d\xi \tag{3a}$$

$$\lambda_{MF} = \frac{2}{b \cdot t \cdot E} \cdot \int_0^\xi Y_M(\xi) \cdot Y_F(\xi)\,d\xi. \tag{3b}$$

Up to the moment of steel yielding or slippage, the local rotation in the cracked cross-section is equal to zero:

$$\phi = \phi^{(M)} + \phi^{(F)} = 0. \tag{4}$$

Equation (4) is the congruence condition giving the unknown force F. Recalling that (Fig. 1):

$$M^* = M - F \cdot (b/2 - h) \tag{5a}$$

$$F^* = -F \tag{5b}$$

eqs (2) and (4) provide:

$$\frac{F \cdot b}{M} = \frac{1}{(0.5 - h/b) + r(\xi)} \tag{6}$$

where:

$$r(\xi) = \frac{\int_0^{\xi} Y_M(\xi) \cdot Y_F(\xi)\, d\xi}{\int_0^{\xi} Y_M^2(\xi)\, d\xi}. \tag{7}$$

If a perfectly plastic behaviour of the reinforcement is considered (yielding or slippage), from eq. (6) the moment of plastic flow for the reinforcement results:

$$M_P = F_P \cdot b \cdot [(0.5 - h/b) + r(\xi)]. \tag{8}$$

However, it should be observed that, if concrete presents a low crushing strength and steel a high yield strength, crushing of concrete can precede plastic flow of reinforcement.

The mechanical behaviour of the cracked reinforced concrete beam section is rigid until the bending moment M_P is exceeded, i.e., $\phi = 0$ for $M \leqslant M_P$. On the other hand, for $M > M_P$ the M–ϕ diagram becomes linear hardening:

$$\phi = \lambda_{MM} \cdot (M - M_P). \tag{9}$$

After the plastic flow of reinforcement, the stress-intensity factor at the crack tip is given by the superposition principle:

$$K_I = K_I^{(M)} + K_I^{(F)}. \tag{10}$$

Recalling eq. (1) and considering the loadings:

$$M^* = M - F_P \cdot (b/2 - h) \tag{11a}$$

$$F^* = -F_P \tag{11b}$$

the global stress-intensity factor results:

$$K_I = \frac{Y_M(\xi)}{b^{3/2} \cdot t} \cdot \left[M - F_P \cdot \left(\frac{b}{2} - h \right) \right] - \frac{F_P}{b^{1/2} \cdot t} \cdot Y_F(\xi). \tag{12}$$

The moment of crack propagation is then:

$$\frac{M_F}{K_{IC} \cdot b^{3/2} \cdot t} = \frac{1}{Y_M(\xi)} + N_P \cdot \left[\frac{Y_F(\xi)}{Y_M(\xi)} + \frac{1}{2} - \frac{h}{b} \right] \tag{13}$$

with:

$$N_P = \frac{f_y \cdot b^{1/2}}{K_{IC}} \cdot \frac{A_S}{A} \tag{14}$$

while the rotation at crack propagation is

$$\phi_F = \lambda_{MM} \cdot (M_F - M_P). \tag{15}$$

The crack propagation moment is plotted in Fig. 2 as a function of the crack depth ξ and varying the brittleness number N_P. For low N_P values, i.e. for low reinforced beams or for small cross-sections, the fracture moment decreases while the crack extends, and a typical phenomenon of unstable fracture occurs. For $N_P \gtrsim 0.7$, a stable branch follows the unstable one, while for $N_P \gtrsim 8.5$ only the stable branch remains. The locus of the minima is represented by a dashed line in Fig. 2. In the upper zone the fracture process is stable whereas it is unstable in the lower one.

Rigid behaviour ($0 \leqslant M \leqslant M_P$) is followed by linear hardening ($M_P < M < M_F$). The latter stops when crack propagation occurs. If the fracture process is unstable, diagram M–ϕ presents a discontinuity and drops from M_F to $F_P \cdot b$ with a negative jump. In fact, in this case, a complete and instantaneous disconnection of concrete occurs. The new moment $F_P \cdot b$ can be estimated according to the scheme in Fig. 3. The non-linear descending law:

$$M = F_P \cdot (b - h) \cdot \cos(\phi/2) \tag{16}$$

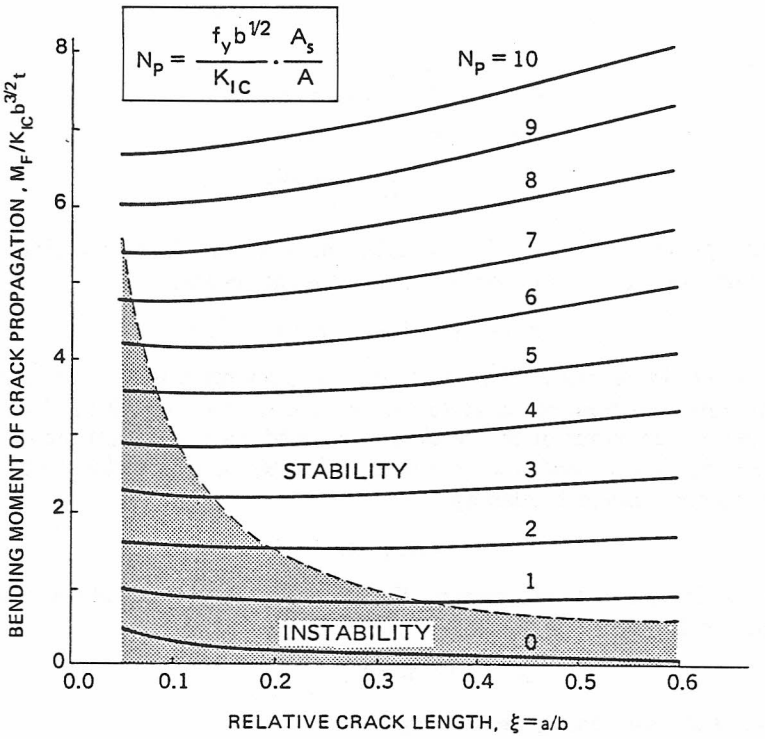

Fig. 2. Bending moment of crack propagation against relative crack length.

is thus approximated by the perfectly plastic one:

$$M = F_P \cdot b. \tag{17}$$

On the other hand, if the fracture process is stable, diagram M–ϕ does not present any discontinuity.

In Fig. 4 the moment–rotation diagrams are reported for $\xi = 0.1$ and five different values of the number N_P. For $N_P \lesssim 0.7$, it is $F_P \cdot b \leqslant M_F$ and therefore a discontinuity appears in the M–ϕ diagram (Fig. 4a–c). On the other hand, for $N_P < 0.7$, the curves in Fig. 2 lie on the unstable zone completely. In conclusion, the above presented theoretical model predicts unstable behaviour for low content of steel and/or for large beam depth.

It is worth noting that the initial crack of the theoretical model was not present in the experimental beams, although a crack formed during the loading process. In addition, the reinforcement plastic flow of the theoretical model, in practice was due also to the steel bar slippage. Nevertheless, the theoretical ductile–brittle transition was confirmed by the experiments, as will be shown in the following sections.

3. MATERIAL PROPERTIES

3.1. *Concrete*

The beams of the present experimental investigation are made of concrete with crushed aggregate of maximum size $D_{max} = 12.7$ mm. The amount of cement (type 525) is 480 kg/m^3, and

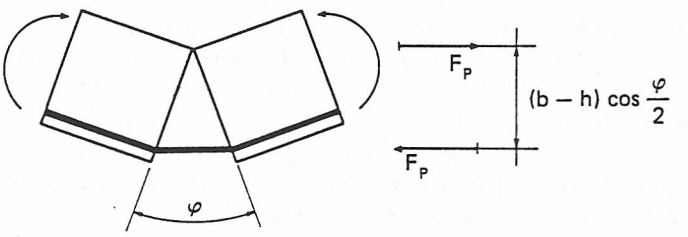

Fig. 3. Statical scheme of complete disconnection of concrete.

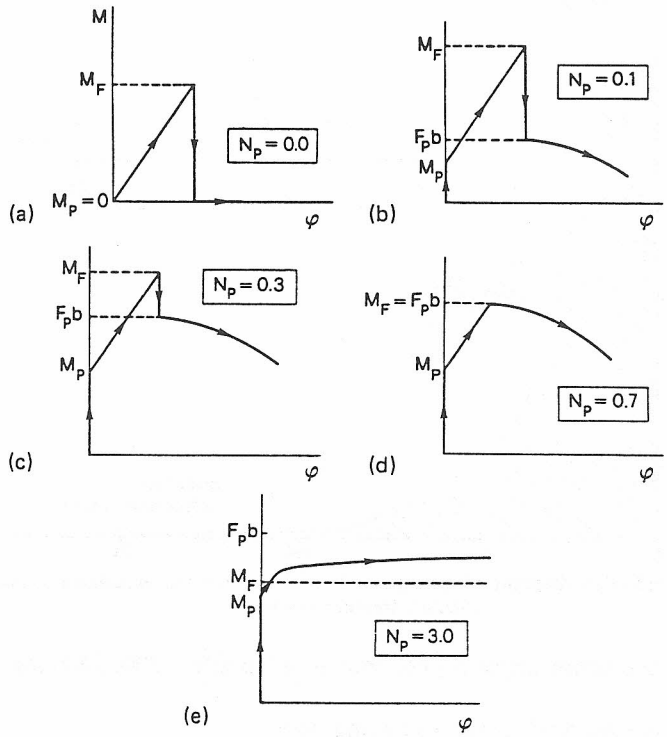

Fig. 4. Ductile–brittle transition in the mechanical behaviour of reinforced concrete beams, by varying the brittleness number, N_p.

the water/cement ratio is equal to 0.27. Considerable attention was spent to avoid cracking due to hydration and shrinkage.

The compressive strength (after 28 days) was obtained with twenty (20) cubic specimens of side 160 mm. The average value resulted to be $R_{cm} = 91.2$ N/mm^2, with a standard deviation of 8.8 N/mm^2.

The curing time of the beams was 3 days at 30°C and then a second period followed at 20°C. As an average, the tests were carried out after 20 days from moulding.

The tests of elastic modulus were performed on three (3) specimens of size 150 × 150 × 450 mm and provided an average value of the secant modulus E (between zero and 1/3 of the ultimate load) equal to 34,300 N/mm^2.

The fracture energy G_F was determined by three point bending testing on three (3) specimens of size $b = 100$ mm, $t = 150$ mm, $l = 750$ mm. The span was equal to $L = 720$ mm and the beams were pre-notched on the center-line, the notch depth being equal to one half of the beam depth ($a/b = 0.5$) and the notch width to 5 mm. The load–deflection diagram for one of the beams tested, is reported in Fig. 5. The average value of the fracture energy results to be $G_F = 0.0484$ N/mm, so that the critical value of the stress-intensity factor can be evaluated:

$$K_{IC} = \sqrt{G_F \cdot E} = 40.75 \text{ N/mm}^{3/2}.$$

3.2. *Steel*

The utilized steel bars present a nominal diameter of 4, 5, 8, 10 mm, respectively. The bars of 4 and 5 mm do not present yielding and the conventional limit, with 0.2% permanent deformation, is equal to 637 N/mm^2 and 569 N/mm^2, respectively. The yield strength for the bars of 8 and 10 mm, on the other hand, is equal to 441 N/mm^2 and 456 N/mm^2, respectively.

4. DESCRIPTION OF THE R.C. BEAM SPECIMENS

Thirty (30) reinforced concrete (R.C.) beams were tested, with the cross-section of thickness $t = 150$ mm and depth $b = 100$, 200, 400 mm. The span between the supports was assumed to be

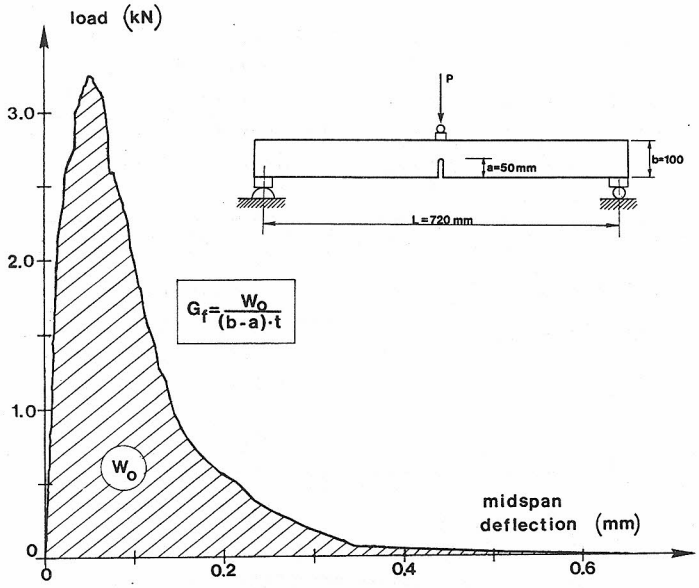

Fig. 5. Load vs deflection diagram of unreinforced specimen, for the experimental determination of concrete fracture energy G_F.

equal to six (6) times the beam depth b and, therefore, to 600, 1200, 2400 mm for the specimens A, B, C, respectively.

The specimens were marked in the following way.

—By varying the beam size:

(A) beam depth $b = 100$ mm ($t = 150$ mm; $L = 600$ mm);
(B) beam depth $b = 200$ mm ($t = 150$ mm; $L = 1200$ mm);
(C) beam depth $b = 400$ mm ($t = 150$ mm; $L = 2400$ mm).

—By varying the brittleness class:

(0) brittleness number $N_P = 0$ (no reinforcement);
(1) brittleness number $N_P \approx 0.13$ (on the average);
(2) brittleness number $N_P \approx 0.36$ (on the average);
(3) brittleness number $N_P \approx 0.72$ (on the average);
(4) brittleness number $N_P \approx 1.18$ (on the average).

The content of steel depends on the beam size and on the brittleness number (see eq. 14). It is reported for each beam in Table 1.

Table 1. Description of the reinforced concrete specimens and related loads of first cracking, steel yielding and final collapse

Beam size	Brittleness class	Sizes $t \times b$ (mm)	Nominal content of steel	Actual percentage of steel	Yield limit of steel (N/mm^2)	Actual value of N_P	Cracking load (kN)	Yielding load (kN)	Ultimate load (kN)
A	0	150 × 100	0	0.00	0	0	11.77	0.00	0.00
	1	150 × 100	1 ϕ 4	0.85×10^{-3}	637	0.134	11.77	7.02	5.78
	2	150 × 100	2 ϕ 5	2.56×10^{-3}	569	0.360	12.50	15.20	11.28
	3	150 × 100	2 ϕ 8	6.53×10^{-3}	441	0.710	13.53	27.94	22.06
	4	150 × 100	2 ϕ 10	10.03×10^{-3}	456	1.170	14.90	34.51	47.81
B	0	150 × 200	0	0.00	0	0	22.55	0.00	0.00
	1	150 × 200	1 ϕ 5	6.40×10^{-4}	569	0.128	19.52	10.29	5.80
	2	150 × 200	3 ϕ 5	1.90×10^{-3}	569	0.380	20.84	23.10	17.14
	3	150 × 200	3 ϕ 8	4.90×10^{-3}	441	0.760	22.36	41.43	56.72
	4	150 × 200	3 ϕ 10	7.75×10^{-3}	456	1.240	26.67	64.95	76.56
C	0	150 × 400	0	0.00	0	0	40.20	0.00	0.00
	1	150 × 400	2 ϕ 4	4.27×10^{-4}	637	0.135	36.67	15.69	8.40
	2	150 × 400	4 ϕ 5	1.28×10^{-3}	569	0.360	38.73	32.36	24.40
	3	150 × 400	4 ϕ 8	3.27×10^{-3}	441	0.720	43.14	53.93	65.00
	4	150 × 400	4 ϕ 10	5.17×10^{-3}	456	1.170	48.93	84.42	97.65

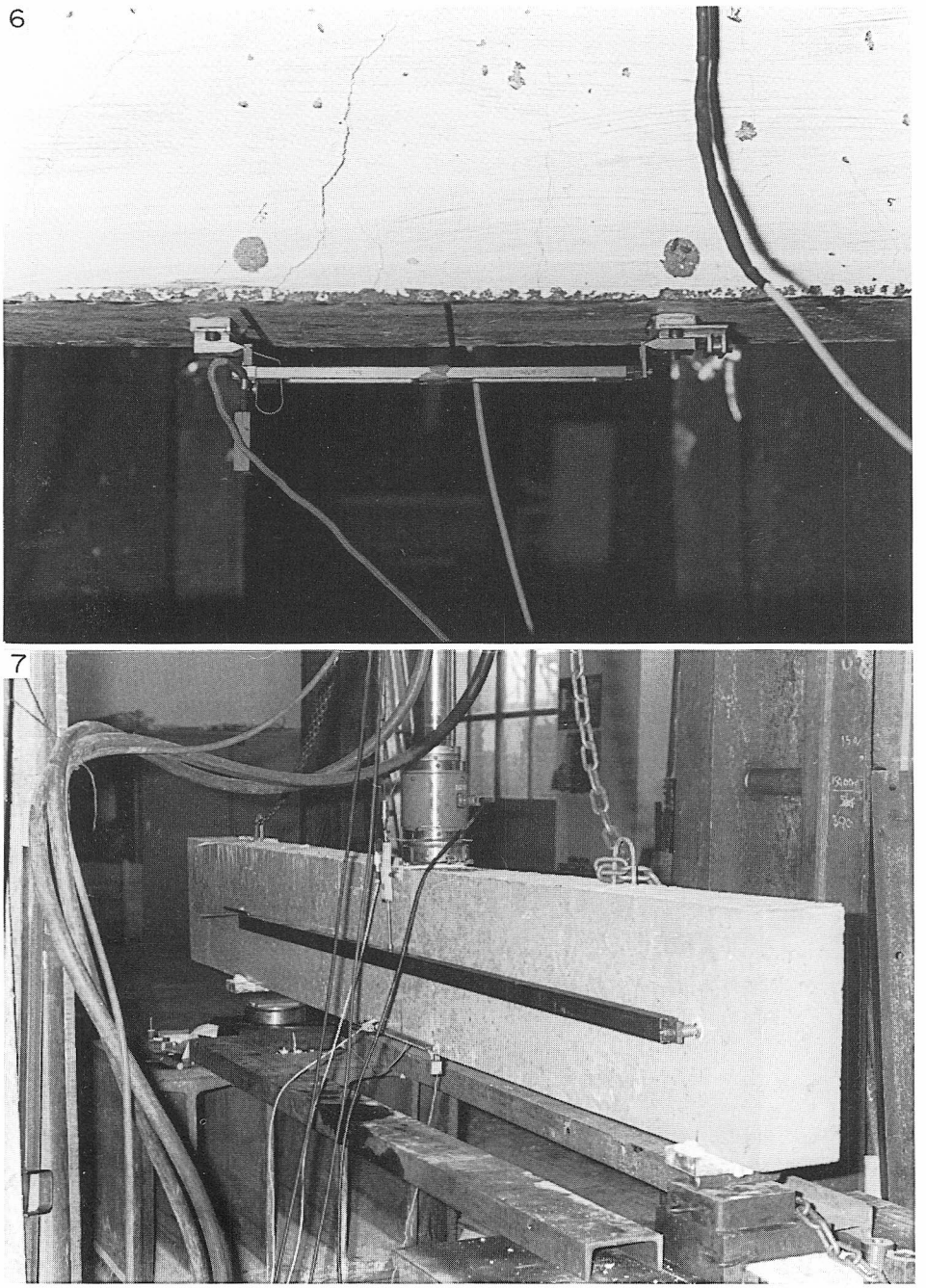

Fig. 6. Strain gauge on the lower beam edge.
Fig. 7. Deflection reference bar connected with the concrete beam.

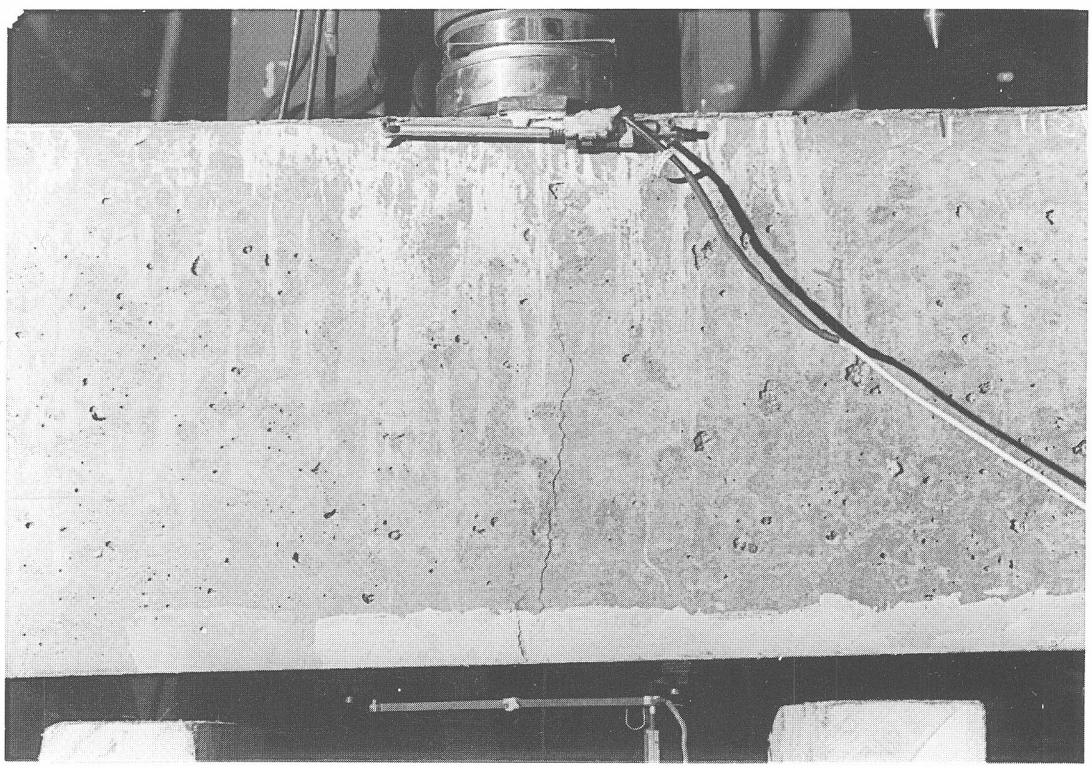

Fig. 8. Brittle enamel applied in the zone where the first crack formation is expected.

The distance of the bars from the lower beam edge is, in each case, equal 1/10 of the beam depth ($h/b = 0.1$). For each beam size (A, B, C) and for each brittleness class (0, 1, 2, 3, 4) two R.C. beams were realized, with a total number of 30 specimens. All the beams were initially unnotched and uncracked. The following results, when not otherwise specified, are related to the average value of each case contemplated by the experimental investigation.

5. TESTING APPARATUS AND PROCEDURE

The experimental investigation was carried out at the Department of Structural Engineering of the Politecnico di Torino. The three point bending tests on R.C. beams were realized by a M.T.S. machine. The beams were supported by a cylindrical roller and a spherical connection, respectively, at the two extremities. The load was applied through a hydraulic actuator and the loading process was controlled by a strain gauge DD1, placed on the lower beam edge, parallel to the beam axis and symmetrical with respect to the force. Its length was equal to the beam depth, i.e. 100, 200 or 400 mm, respectively, for the beam sizes A, B and C (Fig. 6). The sensitivity of the strain gauge utilized is 1 mV/1V/1 mm, for a feed-voltage of 5 V. The strain rate was imposed at a constant and very low value. On the average, the crack formation in the middle of the beam, was achieved after about 7 min and the steel yielding after about 45 min.

Transducers with a sensitivity of 1 mV/0.01 mm were used to measure the central deflection. The latter was referred to a bar, connected with the concrete beam at the middle of the depth and in correspondence of the two supports. Such a device is shown in Fig. 7, for a R.C. beam of depth $b = 400$ mm (size C). Deflection and strain gauge deformation were plotted authomatically as functions of the applied load.

The load of first cracking was detected by means of a brittle enamel, applied in the zone where the first crack formation is expected (Fig. 8). The loads of first crack formation, of steel yielding and of final collapse, are summarized in Table 1.

6. EXPERIMENTAL RESULTS AND DISCUSSION

The load–deflection diagrams are plotted in the Fig. 9(a), (b) and (c), for each beam size and by varying the brittleness class (each curve is related to a single specimen of the two considered). As is possible to verify in Table 1, the peak or first cracking load is decidedly lower than the steel yielding load only in the cases 3 and 4, i.e. for high brittleness numbers N_P. In the cases 0 and 1, the opposite result is clearly obtained. On the other hand, case 2 demonstrates to represent a transition condition between hyperstrength and plastic collapse, the two critical loads being very close. Therefore, the same brittleness transition theoretically predicted in Fig. 4, is reproposed by the experimental diagrams in Fig. 9. The experimental transition value of the brittleness number N_P, results to be between 0.36 and 0.72, whereas the theoretical transition value is approximately equal to 0.70 (Figs 2 and 4).

Specimen C0 ($b = 400$ mm, no reinforcement) presents a very evident snap-back behaviour, the softening branch assuming even a positive slope. It was possible to follow such a branch, since the loading process was controlled by a monotonically increasing function of time, i.e. the crack mouth opening displacement. If the controlling parameter had been the central deflection, a sudden drop in the loading capacity and an unstable and fast crack propagation would have occurred[4–6].

The dimensionless bending moment vs rotation diagrams are plotted in the Fig. 10(a)–(e), for each brittleness class and by varying the beam size. The local rotation is non-dimensionalized with respect to the value ϕ_0 recorded at the first cracking, and is related to the central beam element of length equal to the beam depth b. The bending moment, on the other hand, is non-dimensionalized with respect to concrete fracture toughness K_{IC} and beam depth b (see eq. 13).

The diagrams in Fig. 10 are significant only for $\phi/\phi_0 > 1$, the strain softening and curvature localization occurring only after the first cracking. The dimensionless peak moment does not appear to be the same, when the brittleness class is the same and the beam depth is varying. This is due to the absence of an initial crack or notch. On the other hand, the post-peak branches are very close to each other and present the same shape for each selected brittleness class. The size-scale similarity seems to govern the post-peak behaviour, specially for low brittleness numbers N_P (class

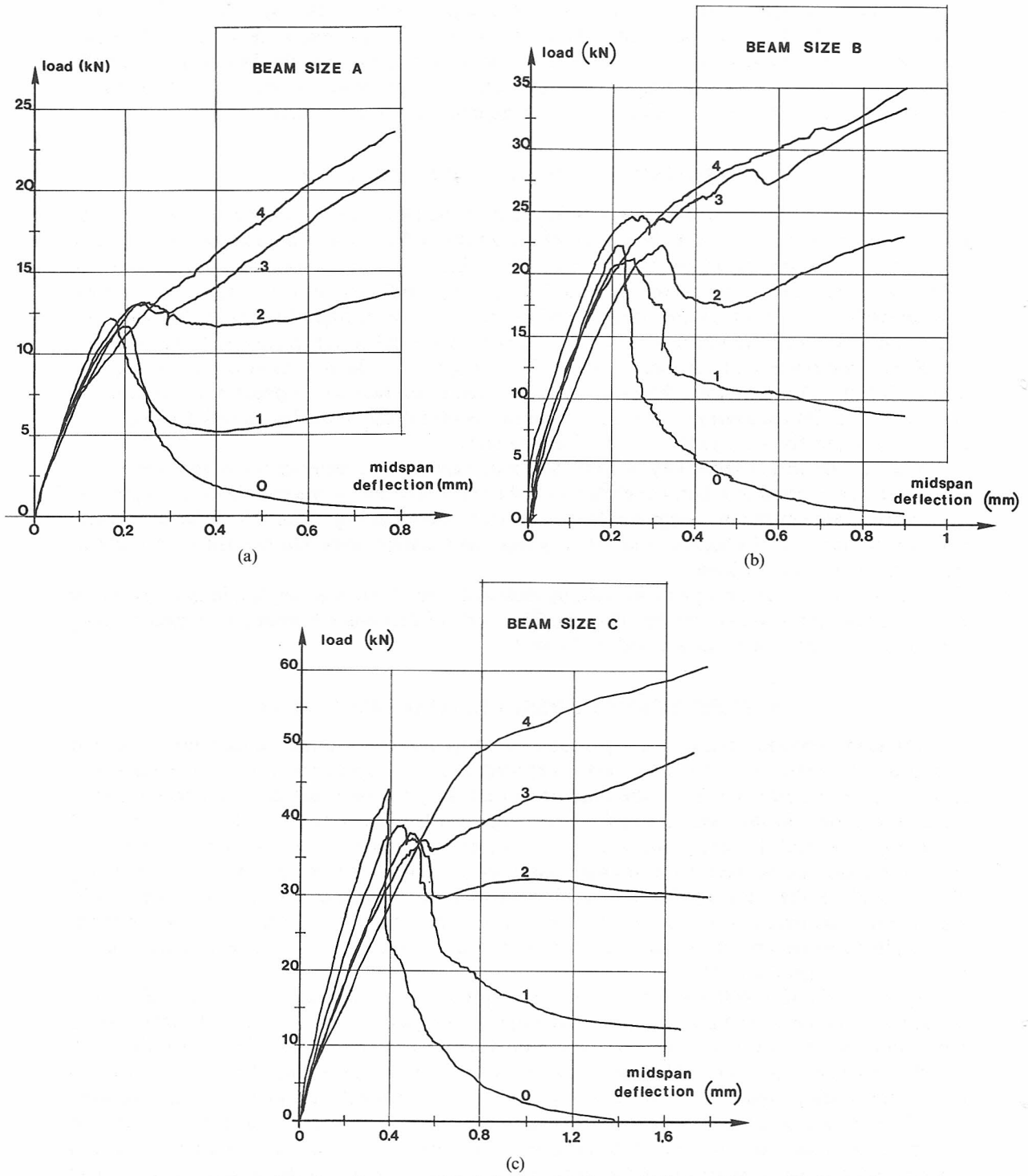

Fig. 9. Load vs deflection diagrams of R.C. beams. (a) Beam depth $b = 100$ mm; (b) beam depth $b = 200$ mm; and (c) beam depth $b = 400$ mm.

0, 1, 2, 3), and for large beam depths b (sizes B, C). In these cases, in fact, it is very likely that the fracture process zone is negligible with respect to the zone where the stress-singularity is dominant, so that the Linear Elastic Fracture Mechanics model (and the non-dimensionalization in Fig. 10) is consistent with the experimental phenomena.

From the present investigation, the demand transpires of analysing the post-peak and ductile behaviour of low reinforced high strength concrete beams[9–12], through the concepts of Fracture

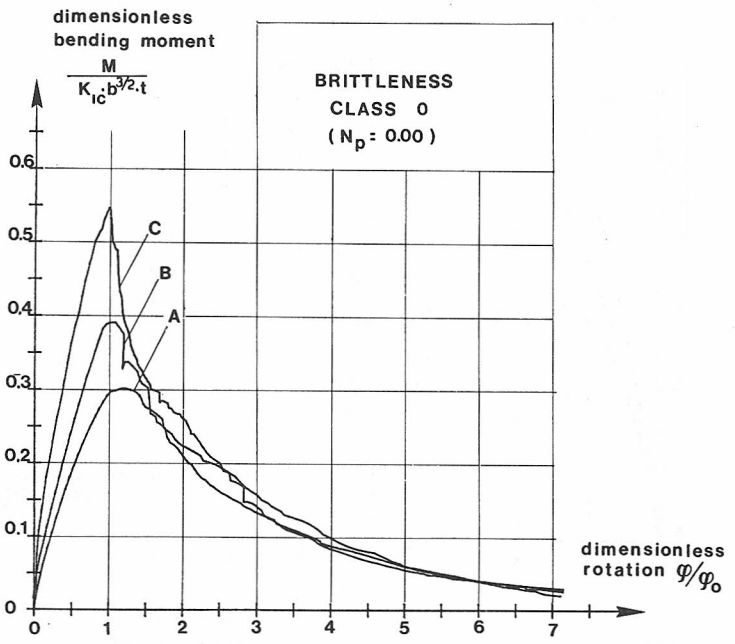

(a)

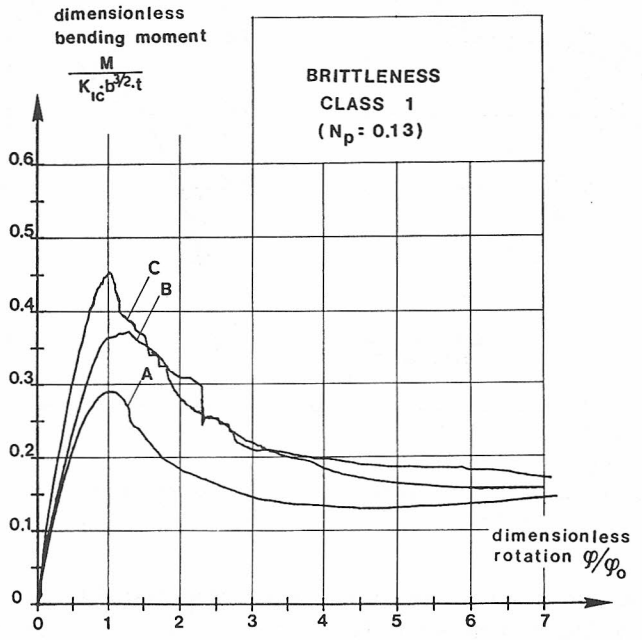

(b)

Fig. 10. (a) and (b).

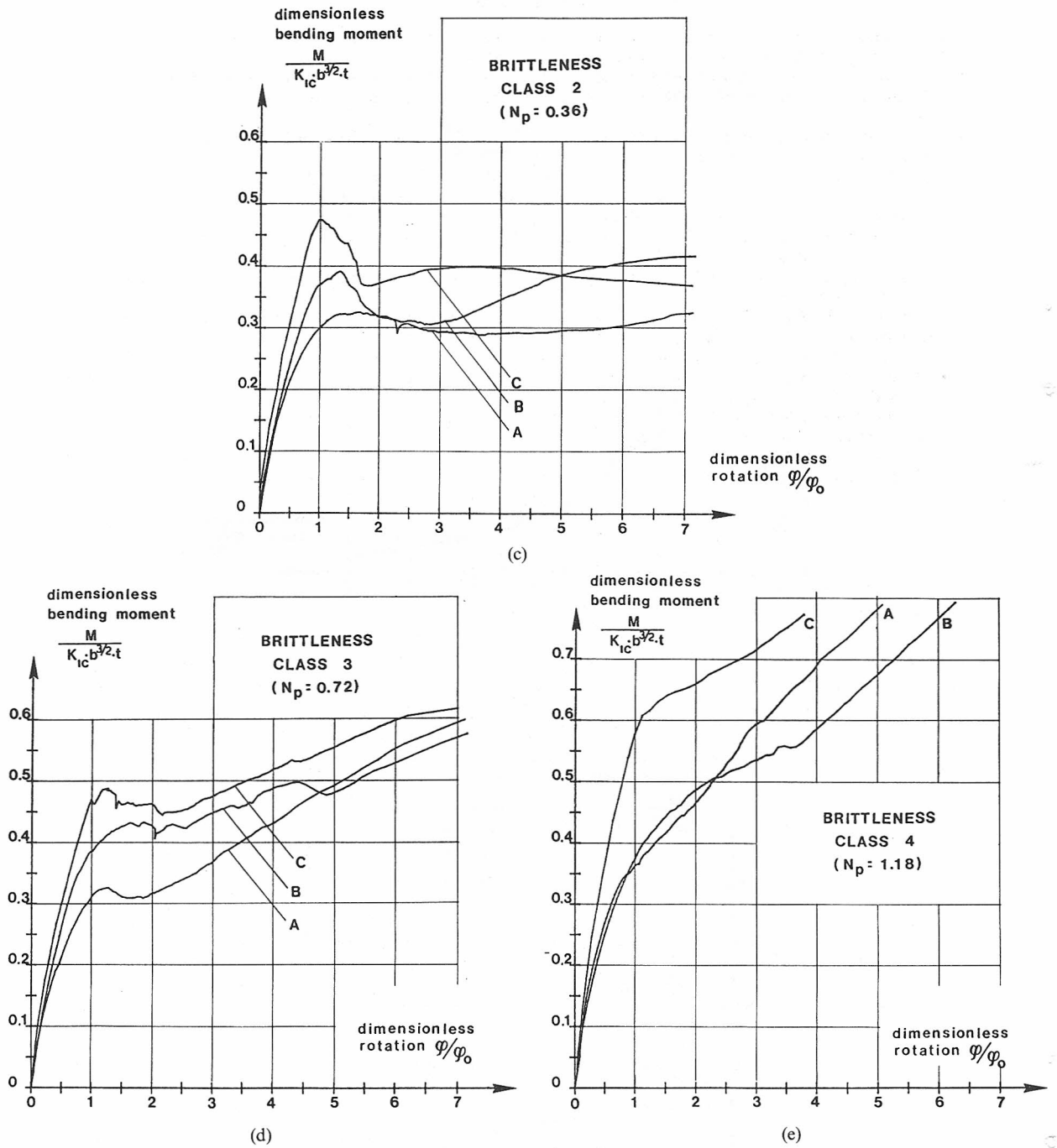

Fig. 10. Dimensionless bending moment vs rotation diagrams. Brittleness number (a) $N_P = 0$; (b) $N_P = 0.13$; (c) $N_P = 0.36$; (d) $N_P = 0.72$; (e) $N_P = 1.18$.

Mechanics. As is demonstrated in the present paper, the possibility of extrapolating predictions from small to large scales, is entrusted to the non-dimensional (brittleness) number N_P (see eq. 14), where, in addition to the traditional geometrical and mechanical parameters, even the concrete fracture toughness K_{IC}, or the concrete fracture energy G_F, appears.

Acknowledgements—The firm RECCHI in Torino, is gratefully acknowledged by the authors for the beam moulding. Thanks are due specially to Geom. Pagani, who attended to the specimens preparation with competence and carefully avoided shrinkage and hydration cracking.

REFERENCES

[1] A. Carpinteri, A fracture mechanics model for reinforced concrete collapse. IABSE Colloquium on Advanced Mechanics of Reinforced Concrete, Delft, pp. 17–30 (1981).
[2] A. Carpinteri, Stability of fracturing process in RC beams. *J. Structural Engng* **110,** 544–558 (1984).
[3] Alberto Carpinteri and Andrea Carpinteri, Hysteretic behaviour of RC beams. *J. Structural Engng* **110,** 2073–2084 (1984).
[4] A. Carpinteri, Interpretation on the Griffith instability as a bifurcation of the global equilibrium. NATO Advanced Research Workshop on Application of Fracture Mechanics to Cementitious Composites, Evanston, Illinois, 4–7 September, 1984 (Edited by S. P. Shah) pp. 287–316. Martinus Nijhoff, The Netherlands (1985).
[5] F. Levi, C. Bosco and P. G. Debernardi, Two aspects of the behaviour of slightly reinforced structures. 25th CEB Plenary Session, Treviso, Italy (11–13 May 1987).
[6] A. Carpinteri, Catastrophical softening behaviour and hyperstrength in low reinforced concrete beams. 25th CEB Plenary Session, Treviso, Italy (11–13 May 1987).
[7] H. Okamura, K. Watanabe and T. Takano, Applications of the compliance concepts in fracture mechanics. *ASTM STP* **536,** 423–438 (1973).
[8] H. Okamura, K. Watanabe and T. Takano, Deformation and strength of cracked members under bending moment and axial force. *Engng Fracture Mech.* **7,** 531–539 (1975).
[9] F. Levi, On minimum reinforcement in concrete structures. *J. Structural Engng* **111,** 2791–2796 (1985).
[10] E. Fehling, G. König and D. Scheidler, Crack width control and tension stiffening. *A. J. Concr. Concr. Struct.* Darmstad Concrete, **1,** 65–86 (1986).
[11] G. König, Restraint crack-width control and minimum reinforcement in thick concrete members. *A. J. Concr. Concr. Struct.* Darmstad Condrete, **1,** 9–22 (1986).
[12] J. P. Jaccoud and H. Charif, Armature Minimal Pour le Contrôle de la Fissuration. Rapport final des essais série "C", Publication IBAP n. 114, Ecole Polytechnique Fédérale de Lausanne, Juillet (1986).

(*Received for publication* 22 *November* 1988)